LIVERPOOL
JOHN MOORES
UNIVERSITY

LJMU Research Online

Tanaka, M, Utsumi, Y, Mazzali, PA, Tominaga, N, Yoshida, M, Sekiguchi, Y, Morokuma, T, Motohara, K, Ohta, K, Kawabata, KS, Abe, F, Aoki, K, Asakura, Y, Baar, S, Barway, S, Bond, IA, Doi, M, Fujiyoshi, T, Furusawa, H, Honda, S, Itoh, Y, Kawabata, M, Kawai, N, Kim, JH, Lee, C-H, Miyazaki, S, Morihana, K, Nagashima, H, Nagayama, T, Nakaoka, T, Nakata, F, Ohsawa, R, Ohshima, T, Okita, H, Saito, T, Sumi, T, Tajitsu, A, Takahashi, J, Takayama, M, Tamura, Y, Tanaka, I, Terai, T, Tristram, PJ, Yasuda, N and Zenko, T

 Kilonova from post-merger ejecta as an optical and near-Infrared counterpart of GW170817

http://researchonline.ljmu.ac.uk/9495/

Article

For more information please contact researchonline@ljmu.ac.uk

http://researchonline.ljmu.ac.uk/

arXiv:1710.05850v1 [astro-ph.HE] 16 Oct 2017

Kilonova from post-merger ejecta as an optical and near-infrared counterpart of GW170817

Masaomi T ANAKA[1], **Yousuke** U TSUMI[2], **Paolo A.** M AZZALI[3,4], **Nozomu** T OMINAGA[5,6], **Michitoshi** Y OSHIDA[7], **Yuichiro** S EKIGUCHI[8], **Tomoki** M OROKUMA[9], **Kentaro** M OTOHARA[9], **Kouji** O HTA[10], **Koji S.** K AWABATA[2], **Fumio** A BE[11], **Kentaro** A OKI[7], **Yuichiro** A SAKURA[11,†], **Stefan** B AAR[12], **Sudhanshu** B ARWAY[13], **Ian A.** B OND[14], **Mamoru** D OI[9], **Takuya** F UJIYOSHI[7], **Hisanori** F URUSAWA[1], **Satoshi** H ONDA[12], **Yoichi** I TOH[12], **Miho** K AWABATA[15], **Nobuyuki** K AWAI[16], **Ji Hoon** K IM[7], **Chien-Hsiu** L EE[7], **Shota** M IYAZAKI[17], **Kumiko** M ORIHANA[12,18], **Hiroki** N AGASHIMA[15], **Takahiro** N AGAYAMA[19], **Tatsuya** N AKAOKA[15], **Fumiaki** N AKATA[7], **Ryou** O HSAWA[9], **Tomohito** O HSHIMA[12], **Hirofumi** O KITA[7], **Tomoki** S AITO[12], **Takahiro** S UMI[17], **Akito** T AJITSU[7], **Jun** T AKAHASHI[12], **Masaki** T AKAYAMA[12], **Yoichi** T AMURA[20], **Ichi** T ANAKA[7], **Tsuyoshi** T ERAI[7], **Paul J.** T RISTRAM[21], **Naoki** Y ASUDA[6] **and** **Tetsuya** Z ENKO[10]

[1]National Astronomical Observatory of Japan, 2-21-1 Osawa, Mitaka, Tokyo 181-8588, Japan
[2]Hiroshima Astrophysical Science Center, Hiroshima University, 1-3-1 Kagamiyama, Higashi-Hiroshima, Hiroshima, 739-8526, Japan
[3]Astrophysics Research Institute, Liverpool John Moores University, IC2, 134 Brownlow Hill, Liverpool L3 5RF, UK
[4]Max-Planck-Institut für Astrophysik, Karl-Schwarzschild-Str. 1, D-85748 Garching bei München, Germany
[5]Department of Physics, Faculty of Science and Engineering, Konan University, 8-9-1 Okamoto, Kobe, Hyogo 658-8501, Japan
[6]Kavli Institute for the Physics and Mathematics of the Universe (WPI), The University of Tokyo Institutes for Advanced Study, The University of Tokyo, 5-1-5 Kashiwa, Chiba 277-8583, Japan
[7]Subaru Telescope, National Astronomical Observatory of Japan, 650 North A'ohoku Place, Hilo, HI 96720, USA
[8]Department of Physics, Toho University, Funabashi, Chiba 274-8510, Japan
[9]Institute of Astronomy, Graduate School of Science, The University of Tokyo, 2-21-1 Osawa, Mitaka, Tokyo 181-0015, Japan
[10]Department of Astronomy, Kyoto University, Kitashirakawa-Oiwake-cho, Sakyo-ku, Kyoto, 606-8502, Japan
[11]Institute for Space-Earth Environmental Research, Nagoya University, Furo-cho, Chikusa, Nagoya, Aichi 464-8601, Japan
[12]Nishi-Harima Astronomical Observatory, Center for Astronomy, University of Hyogo, 407-2, Nishigaichi, Sayo, Hyogo 679-5313, Japan
[13]South African Astronomical Observatory, PO Box 9, 7935 Observatory, Cape Town, South Africa
[14]Institute for Natural and Mathematical Sciences, Massey University, Private Bag 102904 North Shore Mail Centre, Auckland 0745, New Zealand

[15]Department of Physical Science, Hiroshima University, Kagamiyama, Higashi-Hiroshima
    739-8526, Japan
[16]Department of Physics, Tokyo Institute of Technology, 2-12-1 Ookayama, Meguro-ku, Tokyo
    152-8551
[17]Department of Earth and Space Science, Graduate School of Science, Osaka University,
    1-1 Machikaneyama, Toyonake, Osaka 560-0043, Japan
[18]Division of Particle and Astrophysical Science, Graduate School of Science, Nagoya
    University, Furo-cho, Chikusa-ku, Nagoya, 464-8602, Japan
[19]Graduate School of Science and Engineering, Kagoshima University, 1-21-35, Korimoto,
    Kagoshima, 890-0065, Japan
[20]Division of Particle and Astrophysical Science, Graduate School of Science, Nagoya
    University, Furo-cho, Chikusa-ku, Nagoya, 464-8602 Japan
[21]University of Canterbury, Mt John Observatory, PO Box 56, Lake Tekapo 7945, New
    Zealand
[†]Deceased 18 August 2017

Abstract

Recent detection of gravitational waves from a neutron star (NS) merger event GW170817 and identification of an electromagnetic counterpart provide a unique opportunity to study the physical processes in NS mergers. To derive properties of ejected material from the NS merger, we perform radiative transfer simulations of kilonova, optical and near-infrared emissions powered by radioactive decays of r-process nuclei synthesized in the merger. We find that the observed near-infrared emission lasting for > 10 days is explained by 0.03 $M_\odot$ of ejecta containing lanthanide elements. However, the blue optical component observed at the initial phases requires an ejecta component with a relatively high electron fraction (Y_e). We show that both optical and near-infrared emissions are simultaneously reproduced by the ejecta with a medium Y_e of ~ 0.25. We suggest that a dominant component powering the emission is post-merger ejecta, which exhibits that mass ejection after the first dynamical ejection is quite efficient. Our results indicate that NS mergers synthesize a wide range of r-process elements and strengthen the hypothesis that NS mergers are the origin of r-process elements in the Universe.

Key words: Gravitational waves — Stars: neutron — nuclear reactions, nucleosynthesis, abundances

1 Introduction

The first gravitational wave (GW) detection from a neutron star merger was successfully made for GW170817 (Abbott et al. 2017). The detection of GW170817 triggered electromagnetic (EM) observations over the entire wavelength range. Gamma-ray signals were detected about two seconds after the coalescence (Connaughton et al. 2017; Savchenko et al. 2017a). Then, a promising optical and near-infrared counterpart was discovered (Coulter et al. 2017; Allam et al. 2017; Yang et al. 2017, Coulter et al. in prep., Soares-Santos et al. in prep., Valenti et al. in prep.) within a localization area estimated from the three GW detectors (Advanced LIGO Livingston/Hanford and Advanced Virgo). The object, named as SSS17a (or DLT17ck), is located in NGC 4993,

a galaxy at a distance of 40 Mpc. The object was also detected subsequently in ultraviolet (Evans et al. 2017), X-ray (Fong et al. 2017; Troja et al. 2017), and radio (Mooley et al. 2017; Corsi et al. 2017; Hallinan et al. submitted) wavelengths.

Among various EM signals from NS mergers, optical and near-infrared emission is in particular of interest. When two NSs merge, a small part of NS material ($\sim 10^{-3} - 10^{-2} M_\odot$) is ejected into interstellar space (e.g., Rosswog et al. 1999; Ruffert & Janka 2001; Goriely et al. 2011; Hotokezaka et al. 2013; Bauswein et al. 2013). In the ejected material, rapid neutron capture nucleosynthesis (r-process) takes place (e.g., Lattimer & Schramm 1974; Eichler et al. 1989; Korobkin et al. 2012; Wanajo et al. 2014). Then, radioactive decays of r-process nuclei powers EM

emission especially in the optical and near-infrared wavelengths (Li & Paczyński 1998; Kulkarni 2005; Metzger et al. 2010; Kasen et al. 2013; Barnes & Kasen 2013; Tanaka & Hotokezaka 2013). This emission is called "kilonova" or "macronova" (see Fernández & Metzger 2016; Tanaka 2016; Metzger 2017, for reviews).

NS mergers eject material by several mechanisms. The first and robust mechanism is a dynamical mass ejection, which is driven by tidal disruption as well as shock heating. Properties of the dynamical ejecta depend on the mass ratio of two NSs and the equation of state for a NS (e.g., Hotokezaka et al. 2013). After the dynamical ejection, there may also be additional mass ejection ("post-merger" ejecta or "wind" ejecta) by viscous heating and neutrino heating (e.g., Dessart et al. 2009; Fernández & Metzger 2013; Perego et al. 2014; Shibata et al. 2017). However, detailed properties of the post-merger ejecta, such as the ejecta mass, electron fraction (Y_e, number of protons per nucleon which controls the final element abundances), and its spatial distribution, are still unclear due to difficulties in resolving the turbulence and sophisticated treatment of neutrinos in numerical simulations (see e.g., Price & Rosswog 2006; Kiuchi et al. 2014; Giacomazzo et al. 2015; Siegel & Metzger 2017).

The optical and near-infrared counterpart to GW170817, SSS17a, provides an excellent opportunity to study the mass ejection mechanisms of NS mergers and nucleosynthesis in the ejecta. The observed properties of SSS17a are summarized as follows (Utsumi et al. 2017). (1) The optical and near-infrared brightnesses reach absolute magnitudes of -15 or -16 mag (AB magnitude). (2) The optical light curves decline rapidly while the near-infrared light curves evolve more slowly: the flux is dominated by near-infrared light at $t > 5$ days after GW170817 (hereafter t denotes the time after GW170817). (3) The emission at the initial phase ($t < 2$ days) is relatively blue, dominated by the optical light. (4) A non-thermal afterglow component is likely to be negligible since the optical and near-infrared spectra of SSS17a are dominated by a thermal component from the initial phases, at least $t = 1.5$ days (Pian et al. 2017). Utsumi et al. (2017) shows that rapid evolution of SSS17a is consistent with the expection of kilonova models. In this paper, we perform radiative transfer simulations of kilonovae, and study the mass ejection from the NS merger event GW170817.

2 Radiative Transfer Simulations

We perform radiative transfer simulations to calculate light curves and spectra of kilonovae. We use a
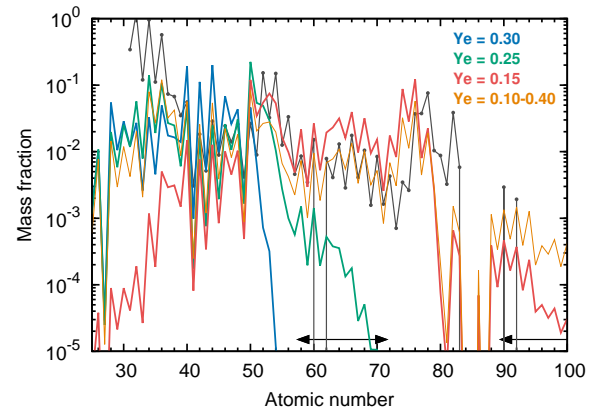

Fig. 1. Element abundances at 1 day after the merger. The blue, green and red lines show the abundance patterns calculated with $Y_e = 0.30$, 0.25, and 0.15, respectively (Wanajo et al. 2014). The abundance patterns of $Y_e = 0.30$ and 0.25 approximate the post-merger ejecta. The orange line shows the abundance by assuming a flat distribution of Y_e from 0.10 to 0.40, which depicts the properties of the dynamical ejecta. The black line shows the solar abundances. The arrows show the lanthanide and actinide elements with high opacities.

wavelength-dependent radiative transfer code (Tanaka & Hotokezaka 2013; Tanaka et al. 2014; Tanaka 2016; Tanaka et al. 2017). For a given ejecta model, i.e., a density structure and element abundances, the code calculates photon transfer by the Monte Carlo method. For a given Y_e (or distribution of Y_e), the code adopts nuclear heating rates by r-process nucleosynthesis calculations by Wanajo et al. (2014). Then, time-dependent thermalization efficiency is taken into account by following the analytic methods presented by Barnes et al. (2016).

A transfer of optical and near-infrared photons is calculated by taking into account bound-bound, bound-free, and free-free transitions and electron scattering. Among them, the bound-bound transitions have a dominant contribution in the optical and near-infrared wavelengths. For the bound-bound transitions, formalism of the expansion opacity (Eastman & Pinto 1993; Kasen et al. 2006) is used as in the previous kilonova simulations (Kasen et al. 2013; Barnes & Kasen 2013; Tanaka & Hotokezaka 2013). For atomic data, we use a line list by Tanaka et al. (2017), which is constructed by the atomic structure calculations for Se ($Z = 34$), Ru ($Z = 44$), Te ($Z = 52$), Nd ($Z = 60$), and Er ($Z = 68$) and supplemented by Kurucz's line list for $Z < 32$ (Kurucz & Bell 1995). Note that since the atomic data include only up to doubly ionized ions, our calculations are applicable only after $t > 0.5$ days, when the temperature is low enough. The number density of each ion is calculated under an assumption of local thermodynamic equilibrium, and populations of excited levels are calculated by assuming the Boltzmann distribution.

For a density distribution in the ejecta, we adopt a sim-
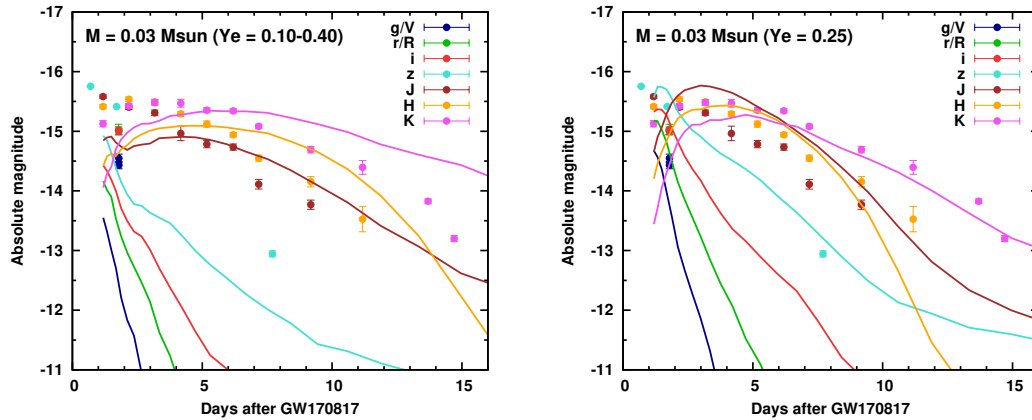
Fig. 2. Optical and near-infrared light curves of SSS17a compared with kilonova models with (left) $Y_e = 0.10 - 0.40$ and (right) $Y_e = 0.25$. The optical and near-infrared data are taken from Utsumi et al. (2017). For the observed data, the line of sight extinction of $E(B - V) = 0.1$ mag has been corrected. All the magnitudes are given in AB magnitudes.

ple power-law form (r^{-3}) from $v = 0.05c$ to $0.2c$, which gives the average velocity of $\langle v \rangle = 0.1c$, as a representative case (Metzger et al. 2010; Metzger 2017). We test three different element abundances, which approximate the dynamical ejecta and post-merger ejecta. The first case depicts the abundances in the dynamical ejecta. Numerical relativity simulations of NS mergers predict wide ranges of Y_e in the dynamical ejecta (Sekiguchi et al. 2015, 2016; Radice et al. 2016; Foucart et al. 2016), which results in a wide elemental distribution from $Z \sim 30$ to 100. Such element abundances are shown in the orange line in Figure 1, which are calculated by assuming a flat Y_e distribution from 0.10 to 0.40 (Wanajo et al. 2014). The second and third cases are for the post-merger ejecta. Since the element abundances are subject to uncertainties, we approximately take two representative values of Y_e: high Y_e ($Y_e = 0.30$, blue line) and medium Y_e ($Y_e = 0.25$, green line). The high Y_e model is completely lanthanide-free while the medium Y_e model contains a small fraction of lanthanide elements. For all the models in this paper, the element distribution in the ejecta is assumed to be spatially homogeneous. Validity of this assumption is discussed in Section 4.

3 Results

The left panel of Figure 2 compares the observed light curves of SSS17a (Utsumi et al. 2017) and the model with $Y_e = 0.10 - 0.40$ (the dynamical ejecta model). We find that the ejecta mass of 0.03 $M_\odot$ reasonably reproduces the near-infrared brightness near the peak. However, the calculated optical light curves are systematically fainter than the observations by 1.0-1.5 mag at the initial phases ($t < 2$ days). This is due to high optical opacities of lan-
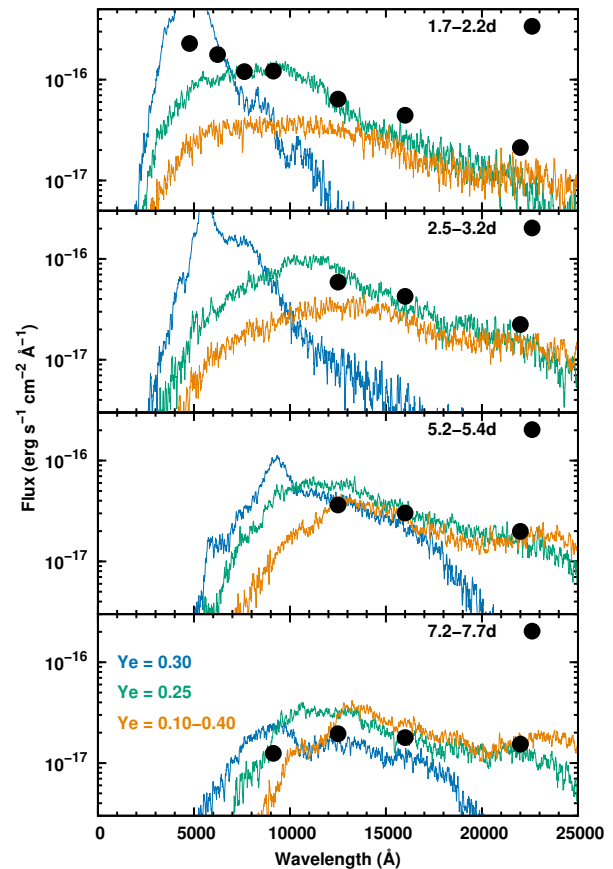
Fig. 3. Time evolution of optical and near-infrared spectral energy distribution of SSS17a compared with three models. The observational data are taken from Utsumi et al. (2017). All of the three models assume the same ejecta mass ($0.03 M_\odot$) and the same average velocity ($\langle v \rangle = 0.1c$). Orange curves show the model of the dynamical ejecta ($Y_e = 0.10-0.40$) while blue and green curves show the models with the elemental abundances calculated with high Y_e ($Y_e = 0.30$) and medium Y_e ($Y_e = 0.25$), respectively.
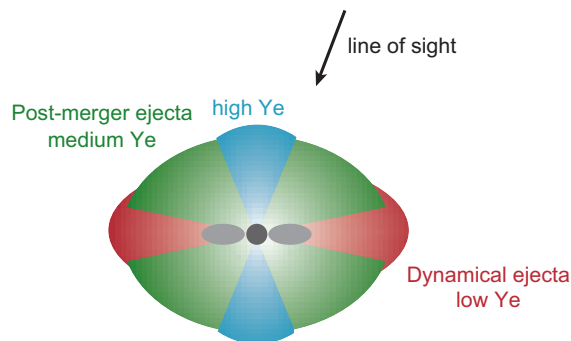
Fig. 4. Schematic picture of the ejecta of the NS merger event GW170817.

thanide elements ($Z = 57 - 71$, Kasen et al. 2013; Barnes & Kasen 2013; Tanaka & Hotokezaka 2013; Fontes et al. 2017; Wollaeger et al. 2017). Because this model has a considerable fraction of lanthanide elements, the resulting kilonova at the initial phases is too red compared with the observations. The faint optical flux is also shown in Figure 3, where the spectral energy distribution of SSS17a is compared with simulated spectra (orange line for $Y_e = 0.10 - 0.40$). To explain the optical brightness, ejecta mass of $\sim 0.06 M_\odot$ is required, although such a model gives too bright near-infrared light curves.

The observed blue emission at the initial phases indicates a presence of the ejecta with relatively low opacities. The green curves in Figure 3 show simulated spectra of the model with the ejecta mass of $0.03 M_\odot$ and $Y_e = 0.25$. The overall agreement between the observed spectral energy distribution and that of the medium Y_e model is satisfactorily well in both the optical and the near-infrared wavelengths from $t = 2$ days to 7 days. As expected from the good agreement with the spectral energy distribution, the model with medium Y_e also reproduces the overall properties of the multi-color light curves (right panel of Figure 2). If the ejecta are completely free from lanthanide elements ($Y_e = 0.30$, blue lines in Figure 3), the spectra are too blue and do not produce enough flux in the near-infrared wavelengths ($> 10,000$ Å) at all the epochs.

4 Discussions

A comparison between our radiative transfer simulations and the observations of SSS17a provides insight on the ejected material in the NS merger event GW170817. We show that the observed near-infrared emission is nicely explained by $0.03 M_\odot$ of ejecta containing lanthanide elements ($Y_e = 0.10 - 0.40$ or $Y_e = 0.25$). However, the model with $Y_e = 0.10 - 0.40$ does not reproduce the blue optical emission at the initial phases. On the other hand, if the ejecta are completely lanthanide free ($Y_e = 0.30$), the

emission is too blue compared with the observations. We find that, as far as a single component model is considered, the model with $Y_e = 0.25$ containing a small fraction of lanthanide elements reproduces both optical and near-infrared emissions reasonably well.

What is the origin of such ejecta? The simulations of the dynamical mass ejection show that a stronger mass ejection occurs when radii of the NSs are smaller (i.e., when the equation of state of the NSs is soft), and thus, shock heating is more efficient. However, a possible maximum mass of the dynamical ejecta is about 0.01 $M_\odot$ with currently available equation of states (e.g., Hotokezaka et al. 2013; Sekiguchi et al. 2015, 2016; Radice et al. 2016). An even higher mass ejection might be possible for a merger with an extreme mass ratio of two NSs. However, in such cases, a tidally disrupted component with low Y_e dominates (see the red line in Figure 1 for the abundances with $Y_e = 0.15$) and the emission would become even redder at the initial phases. By virtue of these facts, it is unlikely that the dynamical ejecta alone can power entire optical and near-infrared emissions of SSS17a.

We suggest that a kilonova from post-merger ejecta plays a dominant contribution for SSS17a. The observed properties are nicely explained if the entire ejecta is moderately lanthanide-rich as in the case of $Y_e = 0.25$. However, it does not necessarily mean that the ejecta should have only a single component. In reality, the ejecta would have an angular distribution of Y_e, having higher Y_e near a polar region (Perego et al. 2014; Fujibayashi et al. 2017). Therefore, more realistic situation may be a combination of spatially separated high, medium, and possibly low Y_e components as illustrated in Figure 4. In fact, the model with medium Y_e does not perfectly reproduce the flux at < 5000 Å at $t = 2$ days and the agreement can be improved with a presence of small amount of high Y_e ejecta probably near the pole. Then, our line of sight may be somewhat off-axis so that we can observe both high and medium Y_e regions. This may also explain the weakness of the gamma-ray emission (Connaughton et al. 2017; Savchenko et al. 2017a; Goldstein et al. 2017; Savchenko et al. 2017b).

Our interpretation implies that a large amount ejecta with medium or high Y_e is ejected during the post-merger phase. The large ejecta mass suggests that the viscous mass ejection is quite efficient in the NS merger event GW170817. A required dimensionless viscous α parameter is $\alpha \gtrsim 0.03$ (Shibata et al. 2017). In addition, we speculate that a relatively long-lived massive NS is present after the merger (Metzger & Fernández 2014; Kasen et al. 2015; Lippuner et al. 2017) so that neutrino emission from the central NS can increase Y_e of the surrounding disk as well

as the ejecta from the disk. It is, however, noted that self-consistent simulations from merger to kilonova are necessary for drawing more quantitative conclusions.

5 Conclusions

We perform the radiative transfer simulations of kilonovae for the optical and near-infrared counterpart of GW170817. We show that the ejecta of 0.03 $M_\odot$ containing lanthanide elements explain the observed near-infrared emissions. However the low-Y_e component alone cannot explain the optical emission at the initial phases. As far as a single component model is considered, the ejecta with medium Y_e (~ 0.25), which contain a small fraction of lanthanide elements, nicely explain both the optical and near-infrared emission simultaneously. We suggest that the post-merger mass ejection plays dominant contribution to the emission.

Our results have implications to the origin of r-process elements. It is known that abundances of r-process elements in Galactic stars show an universal pattern similar to those of the Sun (e.g., Sneden et al. 2008), which implies that a certain phenomenon produces a wide range of r-process elements simultaneously. The observed properties of SSS17a suggest that the NS mergers eject not only dynamical ejecta producing r-process elements beyond the second peak, but also a substantial amount of post-merger ejecta with medium or high Y_e material producing elements from the first to the second peaks. Therefore, the NS mergers seem to synthesize a full range of r-process elements (e.g., Just et al. 2015; Wu et al. 2016). Mass ejection with an order of 0.01$M_\odot$ is also enough to explain the total amount of r-process elements in our Galaxy (e.g., Piran et al. 2014; Hotokezaka & Piran 2015; Rosswog et al. 2017) with the current estimates of the event rate. These strengthen the hypothesis that the NS mergers are the origin of r-process elements in the Universe.

References

Abbott, B. P., et al. 2017, Phys. Rev. Lett., 119, 161101

Allam, S., et al. 2017, GCN Circ., 21530

Barnes, J., & Kasen, D. 2013, ApJ, 775, 18

Barnes, J., Kasen, D., Wu, M.-R., & Martínez-Pinedo, G. 2016, ApJ, 829, 110

Bauswein, A., Goriely, S., & Janka, H.-T. 2013, ApJ, 773, 78

Connaughton, V., et al. 2017, GCN Circ., 21506

Corsi, A., et al. 2017, GCN Circ., 21815

Coulter, D. A., Kilpatrick, C. D., Siebert, M. R., Foley, R. J., J., S. B., Drout, M. R. Simon, J. S., & Piro, A. L. 2017, GCN Circ., 21529

Dessart, L., Ott, C. D., Burrows, A., Rosswog, S., & Livne, E. 2009, ApJ, 690, 1681

Eastman, R. G., & Pinto, P. A. 1993, ApJ, 412, 731

Eichler, D., Livio, M., Piran, T., & Schramm, D. N. 1989, Nature, 340, 126

Evans, P., et al. 2017, GCN Circ., 21550

Fernández, R., & Metzger, B. D. 2013, MNRAS, 435, 502

—. 2016, Annual Review of Nuclear and Particle Science, 66, 23

Fong, W., et al. 2017, GCN Circ., 21786

Fontes, C. J., Fryer, C. L., Hungerford, A. L., Wollaeger, R. T., Rosswog, S., & Berger, E. 2017, arXiv:1702.02990

Foucart, F., O'Connor, E., Roberts, L., Kidder, L. E., Pfeiffer, H. P., & Scheel, M. A. 2016, Phys. Rev. D, 94, 123016

Fujibayashi, S., Sekiguchi, Y., Kiuchi, K., & Shibata, M. 2017, arXiv:1703.10191

Giacomazzo, B., Zrake, J., Duffell, P. C., MacFadyen, A. I., & Perna, R. 2015, ApJ, 809, 39

Goldstein, A., et al. 2017, submitted to ApJ

Goriely, S., Bauswein, A., & Janka, H.-T. 2011, ApJL, 738, L32

Hotokezaka, K., Kiuchi, K., Kyutoku, K., Okawa, H., Sekiguchi, Y., Shibata, M., & Taniguchi, K. 2013, Phys. Rev. D, 87, 024001

Hotokezaka, K., & Piran, T. 2015, MNRAS, 450, 1430

Just, O., Bauswein, A., Pulpillo, R. A., Goriely, S., & Janka, H.-T. 2015, MNRAS, 448, 541

Kasen, D., Badnell, N. R., & Barnes, J. 2013, ApJ, 774, 25

Kasen, D., Fernández, R., & Metzger, B. D. 2015, MNRAS, 450, 1777

Kasen, D., Thomas, R. C., & Nugent, P. 2006, ApJ, 651, 366

Kiuchi, K., Kyutoku, K., Sekiguchi, Y., Shibata, M., & Wada, T. 2014, Phys. Rev. D, 90, 041502

Korobkin, O., Rosswog, S., Arcones, A., & Winteler, C. 2012, MNRAS, 426, 1940

Kulkarni, S. R. 2005, arXiv:astro-ph/0510256

Kurucz, R., & Bell, B. 1995, Atomic Line Data (R.L. Kurucz and B. Bell) Kurucz CD-ROM No. 23. Cambridge, Mass.: Smithsonian Astrophysical Observatory, 1995., 23

Lattimer, J. M., & Schramm, D. N. 1974, ApJL, 192, L145

Li, L.-X., & Paczyński, B. 1998, ApJL, 507, L59

Lippuner, J., Fernández, R., Roberts, L. F., Foucart, F., Kasen, D., Metzger, B. D., & Ott, C. D. 2017, MNRAS, 472, 904

Metzger, B. D. 2017, Living Reviews in Relativity, 20, 3

Metzger, B. D., & Fernández, R. 2014, MNRAS, 441, 3444

Metzger, B. D., et al. 2010, MNRAS, 406, 2650

Mooley, K. P., et al. 2017, GCN Circ., 21814

Perego, A., Rosswog, S., Cabezón, R. M., Korobkin, O., Käppeli, R., Arcones, A., & Liebendörfer, M. 2014, MNRAS, 443, 3134

Pian, E., et al. 2017, Nature, in press

Piran, T., Korobkin, O., & Rosswog, S. 2014, arXiv:1401.2166

Price, D. J., & Rosswog, S. 2006, Science, 312, 719

Radice, D., Galeazzi, F., Lippuner, J., Roberts, L. F., Ott, C. D., & Rezzolla, L. 2016, MNRAS, 460, 3255

Rosswog, S., Feindt, U., Korobkin, O., Wu, M.-R., Sollerman, J., Goobar, A., & Martinez-Pinedo, G. 2017, Classical and Quantum Gravity, 34, 104001

Rosswog, S., Liebendörfer, M., Thielemann, F.-K., Davies, M. B., Benz, W., & Piran, T. 1999, A&A, 341, 499

Ruffert, M., & Janka, H.-T. 2001, A&A, 380, 544

Savchenko, V., et al. 2017a, GCN Circ., 21507

—. 2017b, submitted to ApJ

Sekiguchi, Y., Kiuchi, K., Kyutoku, K., & Shibata, M. 2015, Phys. Rev. D, 91, 064059

Sekiguchi, Y., Kiuchi, K., Kyutoku, K., Shibata, M., & Taniguchi, K. 2016, Phys. Rev. D, 93, 124046

Shibata, M., Kiuchi, K., & Sekiguchi, Y. 2017, Phys. Rev. D, 95, 083005

Siegel, D. M., & Metzger, B. D. 2017, arXiv:1705.05473

Sneden, C., Cowan, J. J., & Gallino, R. 2008, ARA&A, 46, 241

Tanaka, M. 2016, Advances in Astronomy, 2016, 634197

Tanaka, M., & Hotokezaka, K. 2013, ApJ, 775, 113

Tanaka, M., Hotokezaka, K., Kyutoku, K., Wanajo, S., Kiuchi, K., Sekiguchi, Y., & Shibata, M. 2014, ApJ, 780, 31

Tanaka, M., et al. 2017, arXiv:1708.09101

Troja, E., et al. 2017, GCN Circ., 21787

Utsumi, Y., et al. 2017, PASJ, in press

Wanajo, S., Sekiguchi, Y., Nishimura, N., Kiuchi, K., Kyutoku, K., & Shibata, M. 2014, ApJL, 789, L39

Wollaeger, R. T., et al. 2017, arXiv:1705.07084

Wu, M.-R., Fernández, R., Martínez-Pinedo, G., & Metzger, B. D. 2016, MNRAS, 463, 2323

Yang, S., et al. 2017, GCN Circ., 21531

Acknowledgments